

Renormalized Polyakov loops in many representations

Sourendu Gupta*

*Department of Theoretical Physics,
Tata Institute for Fundamental Research,
Homi Bhabha Road, Mumbai 400 005, India*

Kay Hübner†

Physics Department, Brookhaven Natl. Laboratory, Upton, New York 11973, USA

Olaf Kaczmarek‡

Fakultät für Physik, Universität Bielefeld, D-33615 Bielefeld, Germany

(Dated: February 9, 2022)

We present a renormalization procedure for Polyakov loops which explicitly implements the fact that the renormalization constant depends only on the ultraviolet cutoff. Using this we study the renormalized Polyakov loops in all representations upto the **27** of the gauge group $SU(3)$. We find good evidence for Casimir scaling of the Polyakov loops and for approximate large- N factorization. By studying many loops together, we are able to show that there is a matrix model with a single coupling which can describe the high temperature phase of QCD, although it is hard to construct explicitly. We present the first results for the non-vanishing renormalized octet loop in the thermodynamic limit below the $SU(3)$ phase transition, and estimate the associated string breaking distance and the gluelump binding energy. By studying the connection of the direct renormalization procedure with a generalization of an earlier suggestion which goes by the name of the $Q\bar{Q}$ renormalization procedure, we find that they are functionally equivalent.

PACS numbers: 11.10.Gh, 11.10.Wx, 11.15.Ha, 11.15.Pg, 12.38.Gc, 12.38.Mh, 25.75.Nq

I. INTRODUCTION

The proof of confinement in QCD is now literally a million dollar question [1]. There are many ideas about the direction in which such a proof lies. No matter what these ideas are, once they are properly formulated, they are always open to test by lattice techniques. One of the long-lasting ideas has been to examine a toy model of QCD for large number of colors, N [2]. Because of the enhanced symmetry, many quantities become amenable to study in this limit. Computations of corrections upto sub-leading order, $1/N$, have been made for quantities such as hadron masses and pion-nucleon scattering, with intriguing results. Recently, by adding supersymmetries to large- N QCD, very simple toy models have been constructed which are amenable to analytical treatment using the AdS/CFT correspondence [3]. Much excitement has been generated by the plethora of predictions of such toy models, and there have been exciting speculation about their applicability to QCD.

At large N the dynamics of quarks is secondary to that of the gluons, being suppressed by power corrections in N . Hence lattice tests of these ideas have been made in pure gauge, or quenched, QCD. There have been investigations of the string tension and its scaling with N [4], the nature of the phase transition with changing N [5],

and tests of approximate scale-invariance of finite temperature QCD [6]. In this paper we investigate certain ideas about Polyakov loops and their behavior at finite temperature which have developed in recent years based on large N and the AdS/CFT correspondence. We investigate matrix models which could be expected to describe the high temperature phase of pure gauge QCD. Our results put very strong constraints on the kinds of matrix models which may provide a description of pure gauge QCD.

The Polyakov loop is closely connected with confinement since it is the order parameter for the transition from a confined to a deconfined medium. Various models based on Polyakov loops have been proposed to describe the transition to a quark gluon plasma phase and its properties at zero as well as non-zero baryon density [7, 8, 9, 10, 11, 12, 13, 14, 15, 16, 17, 18, 19, 20, 21]. Furthermore the connection of $SU(3)$ theory to the large N limit, in the mean-field approximation, was discussed in [8, 9]. For a test of the reliability and comparison of these Polyakov loop models to pure gauge theory and QCD with dynamical quarks, a detailed knowledge of the behavior of the Polyakov loop in the fundamental and higher representations in those theories is needed.

The Polyakov loop needs to be renormalized, since it has divergent contributions from the ultraviolet. In Section III we present a renormalization procedure which explicitly incorporates properties expected of a good scheme. This direct renormalization technique is naturally applicable to Polyakov loop expectation values in all representations of the color group. The multiplicative renormal-

*Electronic address: sgupta@theory.tifr.res.in

†Electronic address: huebner@bnl.gov

‡Electronic address: okacz@physik.uni-bielefeld.de

izations in different representations are closely connected if the Polyakov loops satisfy a property called Casimir scaling. We present tests of Casimir scaling in Section IV. This leads on, in Section V, to a test of large- N factorization at $N = 3$. We find good evidence for both in a temperature range not too close to T_c .

Next, in Section VI, we examine whether the renormalized Polyakov loops are described in an effective matrix model. By examining the renormalization scheme dependence of these quantities, we find that a single parameter variation of matrix models describes the temperature dependence of the Polyakov loops in various representations. We also show that the matrix model is unlikely to consist of a small set of terms, and therefore hard to construct explicitly from the phenomenology of Polyakov loops.

In Section VII we consider the adjoint Polyakov loop correlations below T_c . We report the first measurement of the renormalized adjoint Polyakov loops in the thermodynamic limit at finite temperature in the confined phase of QCD. We find that aspects of the adjoint Polyakov loop correlations can be summarized in the physics of gluelumps, *i.e.*, colorless states made of static adjoint sources and glue.

In the appendices we consider a renormalization procedure, the $Q\bar{Q}$ procedure, earlier suggested in [22]. We extend it to the renormalization of Polyakov loops in arbitrary representations, consider the relation between the direct and $Q\bar{Q}$ renormalization procedures, and examine “color averaged” Polyakov loop correlators in various representations.

II. DETAILS OF THE CALCULATIONS

We have performed simulations for temperatures up to $24 T_c$ on $N_\sigma^3 \times N_\tau$ lattices with $N_\tau = 4, 6, 8$ and N_σ up to 32 in $SU(3)$ pure gauge theory with the tree level Symanzik-improved gauge action [23, 24]. We used a pseudo heatbath algorithm with FHKP updating in the $SU(2)$ subgroups. Each heatbath update was followed by four overrelaxation steps. The statistics varies from 1000 to 10000 of such sweeps after suitable thermalization. The physical scale has been set using the zero temperature string tension, σ , [25] and a determination of the critical coupling for the deconfinement transition from [26]. We have calculated the Polyakov loops in all representations up to $D = 27$ using the operators defined in (A12)-(A18). The errors on the observables were determined with the Jackknife method.

Furthermore, we have reanalyzed configurations generated using two flavors of staggered quarks with mass $m/T = 0.4$ on a $16^3 \times 4$ lattice at several temperatures above and below the transition temperature [27, 28]. At each temperature we have used statistics of several thousands to calculate Polyakov loops up to $D = 27$.

III. RENORMALIZATION OF POLYAKOV LOOPS

We define the thermal Wilson line, $P(\vec{x})$ at spatial position \vec{x} as

$$P(\vec{x}) \equiv \prod_{i=0}^{N_\tau-1} U_{(\vec{x},i),0}, \quad (1)$$

where $U_{(\vec{x},i),0}$ is the gauge link matrix in the time direction at the point \vec{x} and Euclidean time i . U is a 3×3 matrix which belongs to $SU(3)$. We define the local Polyakov loop as the trace of $P(\vec{x})$,

$$L(\vec{x}) \equiv \text{Tr} P(\vec{x}), \quad (2)$$

where the trace is normalized to one. We denote the expectation value of the Polyakov loop in the fundamental representation of $SU(3)$ by

$$L_3 \equiv \left\langle \frac{1}{V} \sum_{\vec{x}} L(\vec{x}) \right\rangle. \quad (3)$$

Polyakov loops in different representations, L_D , are defined in Appendix A. The subscript D indicates the dimension of the color (irreducible) representation of the Polyakov loop, *e. g.*, L_3 for fundamental or L_8 for adjoint. Expectation values of Polyakov loops are ultraviolet divergent. We will use the superscripts b or r for bare and renormalized Polyakov loop respectively.

A. Basic properties of renormalization

It was pointed out by Polyakov [29] that for smooth loops, ultraviolet divergences can be absorbed in the charge renormalization of gauge fields:

$$L_D^r(T) = (Z_D(g^2))^{\ell(C)} L_D^b(g^2), \quad (4)$$

where $\ell(C)$ is the length of the contour and the coupling, $g^2 = 6/\beta$, on the right is the bare coupling. The quantity on the left is properly renormalized and depends on the renormalized coupling or, through this running coupling, on the temperature. Cusps and self intersections of loops give rise to logarithmic divergences which depend, *e. g.*, on the angle of the cusps [29, 30, 31]. Spatial averages of operators such as $\text{Tr}[L(\vec{x})]^n$, which wind n times around the lattice, also need separate renormalization. Similarly, composite operators such as powers of Polyakov loops, including Polyakov loop susceptibilities, also require independent renormalization.

We have written eq. (4) for an arbitrary representation D . The renormalization constants in different representations, Z_D , can be related to each other if both the bare and the renormalized loops satisfy the relation

$$L_D^{1/C_2(D)} = L_{D'}^{1/C_2(D')}, \quad (5)$$

called Casimir scaling. Here $C_2(D) = \text{Tr} \sum_a \lambda^a \lambda^a$ is the quadratic Casimir operator in the representation D . When Casimir scaling holds, the quantities

$$Z_D(g^2) = [Z_3(g^2)]^{1/d_D}, \quad (6)$$

where $d_D = C_2(D)/C_2(3)$, are all equal. In keeping with the general form in eq. (4) we can write

$$L_D^r(T) = (Z_D(g^2))^{d_D N_\tau} L_D^b(g^2, N_\tau) \quad (7)$$

where the renormalization constants $Z_D(g^2)$ should only depend on the bare coupling. Such a multiplicative renormalization is expected to compensate entirely for the dependence of the bare loop on the cutoff, i.e., the bare coupling, so that the renormalized loop on the left is a function only of the temperature. Furthermore, if Casimir scaling is found to hold, then all the Z_D collapse to a single function $Z_3(g^2)$, i.e. loops in all representations can be simultaneously renormalized. Note that there is one remaining ambiguity: the function $Z_3(g^2)$ can be multiplied by a single coupling independent constant without affecting the renormalization. Thus, a one parameter family of renormalization schemes for Polyakov loops is defined by eq. (7).

B. Direct renormalization of the Polyakov loop

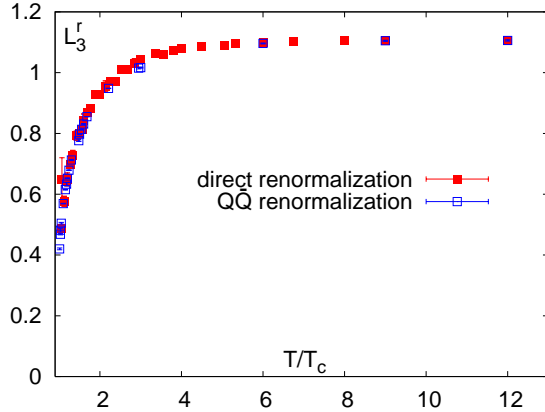


FIG. 1: Comparison of the renormalized Polyakov loop in the fundamental representation, $L_3^r(T)$, obtained with the two different renormalization procedures.

In this subsection we present a complete renormalization procedure which implements eq. (7). We call this the direct renormalization prescription. A similar procedure was discussed earlier in [32]. Denote by $L_D(g^2, N_\tau)$ the Polyakov loop expectation value obtained after taking the thermodynamic limit at a temperature $T = 1/a(g^2)N_\tau$, where a is the lattice spacing at a bare coupling g^2 and N_τ is the temporal extent of the lattice.

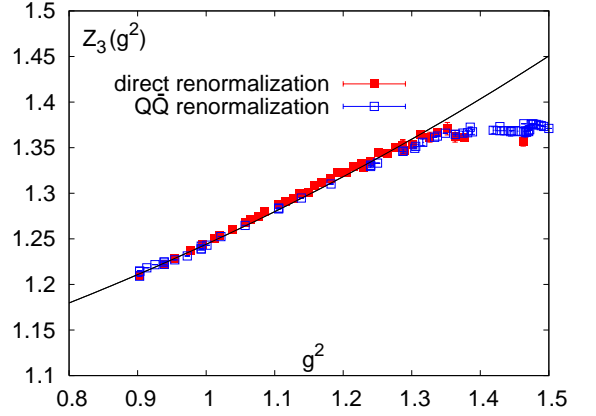


FIG. 2: Comparison of the renormalization constants for fundamental loops, $Z_3^R(g^2)$, for the two different renormalization procedures. g^2 denotes the bare coupling and the solid line is the same as in fig. 4.

We will describe the procedure for a fundamental loop first.

First choose the value of $L_3^r(T_{ref})$, at a reference temperature T_{ref} . It is clear from eq. (7) that this choice is exactly equivalent to fixing the renormalization scheme. It is convenient, but not necessary, to take T_{ref} to be the maximum temperature in the study: in our case $T_{ref} = 12T_c$. We discuss our choice of scheme in Appendix C. This sets the first step of the iterative procedure starting at the initial temperature $T_1 = T_{ref}$. Next we need measurements at (at least) two different temporal extents, N_τ^α and N_τ^β , say, with $N_\tau^\alpha > N_\tau^\beta$, both at the temperature T_i (we begin with $i = 1$ and set up an iteration). Therefore these measurements correspond to two different lattice cutoffs $a(g_{i,\alpha}^2)N_\tau^\alpha = a(g_{i,\beta}^2)N_\tau^\beta$ with $a_{i,\alpha} < a_{i,\beta}$, where the subscripts are self-explanatory. We obtain two different renormalization constants,

$$(Z_3(g_{i,\alpha}^2))^{N_\tau^\alpha} L_3^b(g_{i,\alpha}^2, N_\tau^\alpha) = L_3^r(T_i), \quad (8)$$

$$(Z_3(g_{i,\beta}^2))^{N_\tau^\beta} L_3^b(g_{i,\beta}^2, N_\tau^\beta) = L_3^r(T_i). \quad (9)$$

The third step is to advance the iteration. We do this by making a measurement of $L_3^b(g_{i,\beta}^2, N_\tau^\alpha)$ on the lattice with temporal extent N_τ^α at a temperature $T_{i+1} = 1/a_{i,\beta}N_\tau^\alpha = (N_\tau^\beta/N_\tau^\alpha)T_i$. Since the renormalization constant is already known from eq. (9), one obtains the value of $L_3^r(T_{i+1})$

$$L_3^r(T_{i+1}) = (Z_3(g_{i,\beta}^2))^{N_\tau^\alpha} L_3^b(g_{i,\beta}^2, N_\tau^\alpha). \quad (10)$$

Since we have the value of the renormalized loop at a new temperature, we can now iterate the procedure from the second step on. The iteration gives the renormalized loops and the renormalization constants at a decreasing series of temperatures.

Four points about the prescription are worth noting explicitly. First, the procedure extends without change to

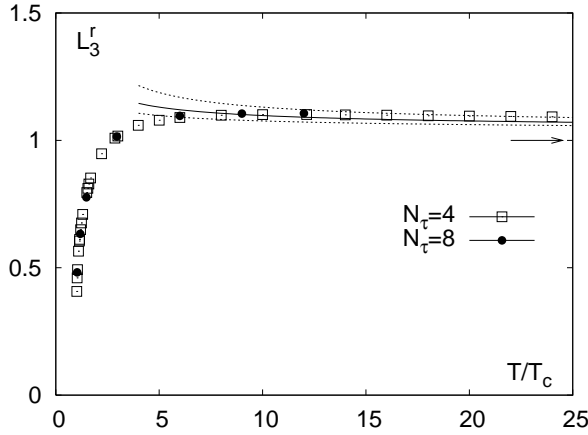


FIG. 3: The renormalized fundamental Polyakov loop in SU(3) pure gauge theory for two values of the temporal lattice extent N_τ . The lines show the perturbative result (11) and are explained in the text. The arrow represents the asymptotic high temperature limit, $L_3^r = 1$.

any representation D . The test of Casimir scaling would be to assume that the bare loops in different representations at T_{ref} are related by eq. (5), and then check whether the renormalized loops at all T are related in the same way. We discuss this further in Section IV. Second, in the confined phase of the pure gauge theory the bare Polyakov loop, in any representation with non-vanishing triality, vanishes in the thermodynamic limit; as a result the direct renormalization procedure can only be used above T_c for such representations. Third, a reverse iteration can always be performed by choosing $T_{i+1} = 1/a_{i,\alpha} N_\tau^\alpha = (N_\tau^\alpha/N_\tau^\beta) T_i > T_i$. Finally, although we discussed the procedure for two values of N_τ , it can be easily extended to a larger number of values for the temporal extent.

The renormalized Polyakov loop in the fundamental representation obtained by the direct procedure described here is shown in Figure 1. Also shown, for comparison, are the results obtained from a completely different renormalization procedure [22] based on a matching of the short distance behavior of heavy quark-antiquark free energies to the zero temperature potential (labeled as $Q\bar{Q}$ -renormalization). Both these procedures allow a one parameter family of renormalization schemes, and the schemes have been chosen so that the value of $L_3^{(r)}(T_{ref})$ match. Figure 2 shows the results for the renormalization constant. These figures indicate the functional equivalence of the two renormalization procedures.

C. Fundamental Polyakov loops

We have extended previous measurements of the fundamental Polyakov loop [22] to temperatures as high as

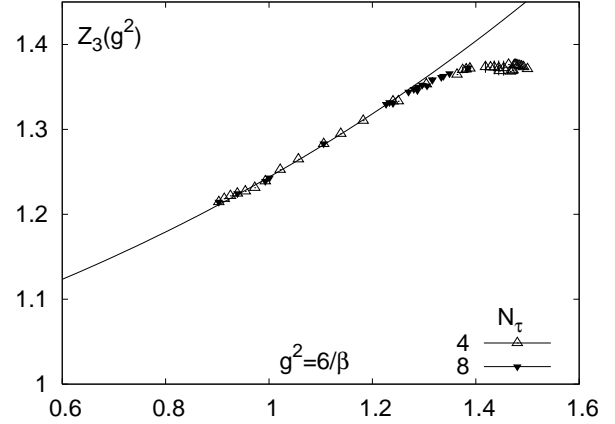


FIG. 4: The renormalization constants $Z_3(g^2)$ as a function of the bare coupling $g^2 = 6/\beta$ calculated on lattices of size $32^3 \times N_\tau$ with $N_\tau = 4$ and 8. The line comes from a fit to (13) as explained in the text.

N_τ	T/T_c	L_3^r	N_τ	T/T_c	L_3^r
4	1.012	0.4070(11)	4	6.001	1.0897(4)
4	1.031	0.4600(7)	4	8.002	1.0986(5)
4	1.049	0.4927(22)	4	10.00	1.1011(7)
4	1.099	0.5649(14)	4	12.13	1.1014(6)
4	1.144	0.6049(3)	4	14.00	1.1000(3)
4	1.151	0.6114(16)	4	16.00	1.0988(6)
4	1.200	0.6494(12)	4	18.01	1.0966(5)
4	1.241	0.6759(15)	4	20.00	1.0954(8)
4	1.301	0.7095(13)	4	22.00	1.0939(10)
4	1.499	0.7953(13)	4	24.00	1.0924(12)
4	1.549	0.8115(8)			
4	1.600	0.8288(9)	8	1.03	0.4818(99)
4	1.684	0.8523(2)	8	1.18	0.6330(125)
4	2.214	0.9475(3)	8	1.48	0.7763(116)
4	2.858	1.0087(1)	8	2.95	1.0149(68)
4	2.999	1.0169(1)	8	6.00	1.0961(33)
4	3.987	1.0591(2)	8	9.00	1.1049(27)
4	5.001	1.0791(2)	8	12.00	1.1060(26)

TABLE I: The renormalized fundamental Polyakov loop $L_3^r(T)$ obtained on lattices of size $32^3 \times N_\tau$ with $N_\tau = 4$ and 8. T/T_c denotes the temperature in units of the critical temperature.

$24T_c$. The results for $L_3^r(T)$ are shown in Figure 3 and listed in Table I. The corresponding renormalization constants are plotted in Figure 4 and listed in Table II. The direct renormalization procedure for the fundamental Polyakov loop stops at g^2 corresponding to T_c on the lattice with the smallest N_τ . Since the $Q\bar{Q}$ procedure gives identical results upto this point, and can be continued to larger g^2 , the tables contain results obtained

N_τ	g^2	Z_3	N_τ	g^2	Z_3
4	0.90294	1.2144(2)	4	1.47783	1.3759(1)
4	0.91348	1.2183(3)	4	1.48148	1.3754(1)
4	0.92531	1.2217(2)	4	1.48515	1.3748(1)
4	0.93869	1.2245(3)	4	1.48883	1.3742(1)
4	0.95426	1.2270(2)	4	1.49254	1.3733(1)
4	0.97248	1.2312(1)	4	1.50000	1.3711(1)
4	0.99282	1.2389(2)			
4	1.02157	1.2525(1)	8	0.90294	1.2145(2)
4	1.05684	1.2648(1)	8	0.93882	1.2246(2)
4	1.10577	1.2829(2)	8	0.99282	1.2391(2)
4	1.13889	1.2948(1)	8	1.00117	1.2431(1)
4	1.18227	1.3102(2)	8	1.10577	1.2833(2)
4	1.23993	1.3330(13)	8	1.22647	1.3297(21)
4	1.25000	1.3331(2)	8	1.23302	1.3319(23)
4	1.30435	1.3531(9)	8	1.23985	1.3307(2)
4	1.36364	1.3646(1)	8	1.26995	1.3441(36)
4	1.37457	1.3700(39)	8	1.28003	1.3473(33)
4	1.38857	1.3717(47)	8	1.28703	1.3459(1)
4	1.41878	1.3734(68)	8	1.28742	1.3496(31)
4	1.42857	1.3731(2)	8	1.29618	1.3523(29)
4	1.43575	1.3730(80)	8	1.30574	1.3514(1)
4	1.44439	1.3724(87)	8	1.31579	1.3585(26)
4	1.45384	1.3721(88)	8	1.31602	1.3583(28)
4	1.46699	1.3681(8)	8	1.33333	1.3614(2)
4	1.47059	1.3690(2)	8	1.33743	1.3628(3)
4	1.47420	1.3757(2)	8	1.34916	1.3659(3)
4	1.47601	1.3761(1)	8	1.38530	1.3724(2)

TABLE II: The renormalization constants for the fundamental Polyakov loop, $Z_3(g^2)$ obtained on lattices of size $32^3 \times N_\tau$ with $N_\tau = 4$ and 8. $g^2 = 6/\beta$ denotes the bare coupling.

using this procedure.

The Polyakov loop for SU(N) pure gauge theory in HTL perturbation theory [33] is

$$L_D = 1 + 2\pi^2 C_2(D) \left\{ \left(\frac{2}{3}N \right)^{\frac{1}{2}} \left(\frac{g^2}{8\pi^2} \right)^{\frac{3}{2}} + N \left(\frac{g^2}{8\pi^2} \right)^2 \times \left(\ln \left(\frac{g^2}{8\pi^2} \right) + \ln \left(\frac{2\pi^2 N}{3} \right) + \frac{3}{2} \right) \right\}. \quad (11)$$

With an appropriate running coupling, $g(T)$, this defines the renormalized Polyakov loop up to $\mathcal{O}(g^4)$. We make the specific choice of the two-loop formula,

$$g^{-2}(T) = 2\beta_0 \ln \left(\frac{\mu T}{\Lambda_{\overline{MS}}} \right) + \frac{\beta_1}{\beta_0} \ln \left(2 \ln \left(\frac{\mu T}{\Lambda_{\overline{MS}}} \right) \right), \quad (12)$$

with $\beta_0 = 11/(16\pi^2)$ and $\beta_1 = 102/(16\pi^2)^2$. and $T_c/\Lambda_{\overline{MS}} = 1.14$. [34, 35, 36]. These predictions are shown in Figure 3 for the choices $\mu = \pi/2$, π and 2π .

Due to the phase transition, the Polyakov loop expectation value vanishes below T_c and rises beyond $5T_c$. It starts to decrease from about $10T_c$ and approaches the asymptotic high temperature limit, $L_3^r = 1$ (indicated by the arrow in fig. 3), from above, in qualitative agreement with weak coupling theory. The lattice measurements seem to fall a little slower than the HTL prediction, upto the highest temperature examined. Approximate qualitative agreement with HTL perturbation theory, without exact quantitative agreement upto very high temperature has been seen in many other contexts in high temperature QCD, most notably for screening masses [37, 38] at high temperatures.

The comparison of the renormalization constants $Z_3(g^2)$ for different N_τ , shown in Figure 4 demonstrates that Z_3 depends only on the bare coupling, and not on temperature. The solid line in Fig. 4 shows the result of a fit with a (two-loop) perturbation theory [39] inspired Ansatz,

$$Z_3(g^2) = \exp \left(g^2 \frac{N^2 - 1}{N} Q^{(2)} + g^4 Q^{(4)} \right) \quad (13)$$

where $Q^{(2)}$ and $Q^{(4)}$ are expected to be independent of N_τ if eq. (7) is to be satisfied. Although we are in coupling range which is not small enough for the weak coupling expansion to be numerically accurate, the fit works surprisingly well. In fact the bare coupling becomes significantly larger than unity before this ansatz begin to overestimate the actual values of Z_3 . From the best fit analysis with a fit range $g^2 \lesssim 1.2$ we obtained the values $Q^{(2)} = 0.0591(21)$ and $Q^{(4)} = 0.0605(54)$. Interestingly, although our computations are done using a Symanzik improved action, the value of $Q^{(2)}$ agrees reasonably well with result from lattice perturbation theory, $Q^{(2)} = 0.057(2)$ [39], using the Wilson action. The renormalization scheme dependence of these results will be discussed in Appendix C.

D. Polyakov loops in other representations

The results for the measured bare Polyakov loops is shown in fig. 5 for the representations $D = 3$ to $D = 15$. The renormalization of Polyakov loops in each representation, D , was obtained using the direct renormalization procedure. For each D , the starting point was taken at $T_{ref} = 12T_c$. We fixed the scheme through the choice

$$L_D^r(T_{ref}) = (L_3^r(T_{ref}))^{d_D}. \quad (14)$$

Except for this assumption at a single temperature, the renormalization was performed independently at each D . Since the loops were measured at arbitrary temperature values, spline interpolations (solid lines) for the data sets were used in the renormalization iteration. The errors on renormalized Polyakov loops and renormalization constants were obtained through a jackknife analysis. The accumulation of errors during iteration, the exponential

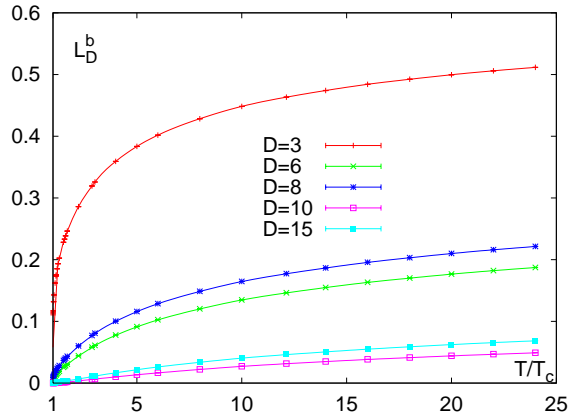


FIG. 5: The (bare) Polyakov loops for different representations D measured on $32^3 \times 4$ lattices. The solid lines are the splines used in our analysis to extract the renormalization constants in the direct renormalization procedure.

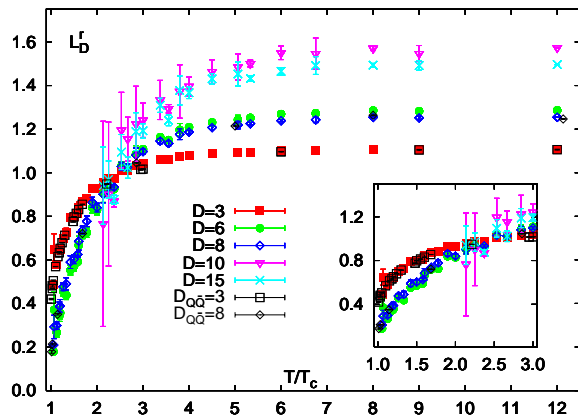


FIG. 6: The renormalized Polyakov loops for different representations D obtained with the direct renormalization procedure. Also shown are the results obtained from the $Q\bar{Q}$ -method for fundamental and adjoint loops, labeled $D_{Q\bar{Q}}$.

d_D in (7), and the larger statistical errors for higher representations lead to large errors in the renormalization procedure for representations higher than $D = 8$ as one approaches T_c .

The results for $L_D^r(T)$ are shown in Figure 6. For comparison we have also included in the figure the results for the fundamental and adjoint representation obtained with the $Q\bar{Q}$ procedure (see Appendix B). These agree within errors, demonstrating again that the two renormalization procedures give equivalent results.

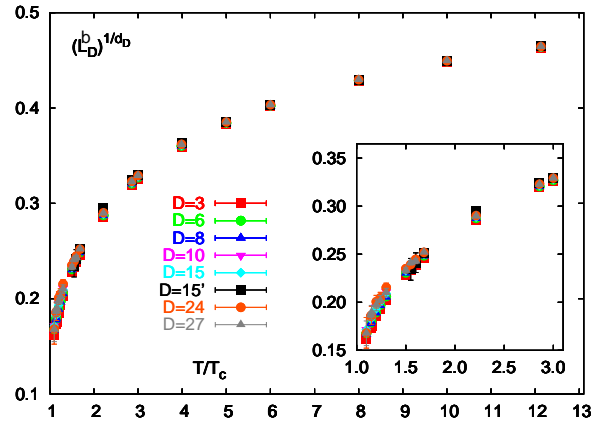


FIG. 7: The Casimir-scaled bare Polyakov loops for different representations D measured on $32^3 \times 4$ lattices.

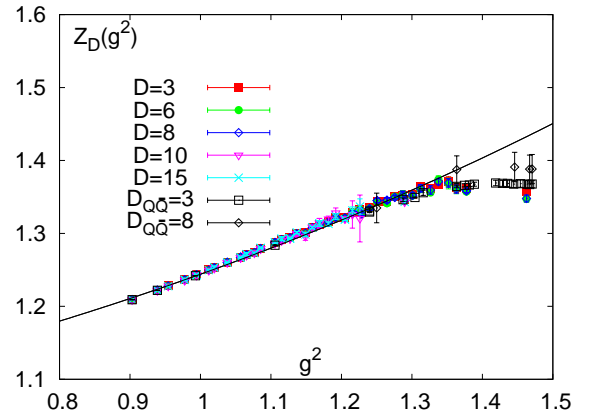


FIG. 8: The renormalization constants for different representations D obtained with the direct renormalization procedure. Also shown are the results obtained from the $Q\bar{Q}$ -method for fundamental and adjoint loops.

IV. CASIMIR SCALING

In [40] it was shown that Casimir scaling is realized in perturbation theory (at least) up to two-loop order, $\mathcal{O}(g^4)$. This statement even holds for QCD with (massless) dynamical quarks as shown in lattice perturbation theory in [41]. Moreover, lattice calculations at finite temperature employing an effective action for the Polyakov loop in SU(3) have found Casimir scaling to be realized for the Polyakov loop as well [42]. Numerical calculations on the lattice at $T = 0$ in SU(3) pure gauge theory show that Casimir scaling is realized also in the non-perturbative regime for distances smaller than the string breaking distance [43]. The very good agreement of the lattice data with the Casimir scaling hypothesis at non-perturbative distances in the vacuum has considerable ramifications on models for non-perturbative QCD,

especially for the confinement mechanism [44].

We have noted before that if Casimir scaling holds, then it holds for bare as well as renormalized loops. Since bare loops have smaller statistical errors, we test Casimir scaling through these. The most straightforward test is to note that $(L_D^b)^{1/d_D}$ must be independent of D if Casimir scaling holds. In Figure 7 we show that deviations from Casimir scaling are visible only very close to T_c . This has implications for weak coupling expansions. Beyond two-loop order in a perturbative series of the Polyakov loop, Casimir scaling violations can appear [40]. These must be strongly suppressed compared to contributions which scale with the quadratic Casimir operator.

An equivalent test is to note that the quantities $Z_D(g^2)$ which are obtained using the assumption in eq. (14) are equal within errors, as shown in Figure 8. Note that this agreement is an outcome of the renormalization procedure, and not built into it. A finer test of Casimir

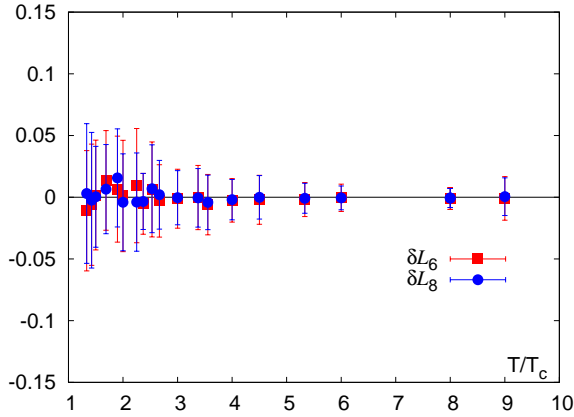


FIG. 9: Difference loops for the sextet, δL_6 , and adjoint, δL_8 , Polyakov loops using Casimir scaling (15).

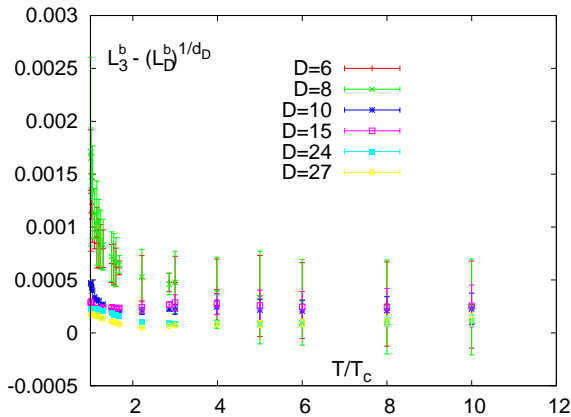


FIG. 10: Difference loops for all representation, δL_D , using Casimir scaling (15).

scaling is obtained using the difference loops

$$\delta L_D = L_3 - (L_D)^{1/d_D}, \quad (15)$$

The results for the renormalized difference loops for $D = 6$ and 8 are shown in Figure 9. They are consistent with zero at all temperatures. For the higher representations a statistically finer test is obtained with bare loops, since the errors on the renormalized loops are large. The results are shown in Figure 10. Even here, Casimir scaling is a good approximation, which gets better the higher the temperature.

A. Two-flavor QCD

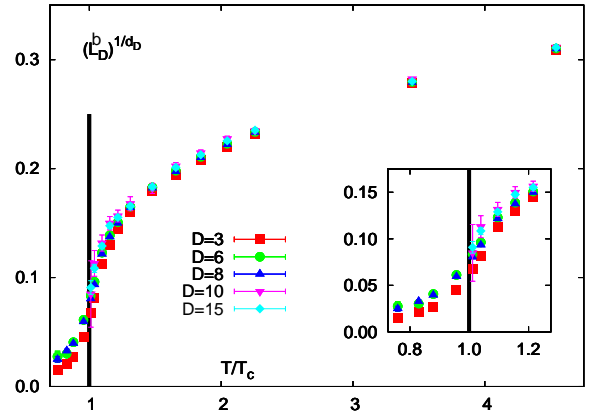


FIG. 11: Testing Casimir scaling for the bare Polyakov loop in 2-flavor QCD $\langle L_D \rangle$ from a $16^3 \times 4$ lattice for all $D = 3, 6, 8, 10, 15$.

It is interesting to check whether Casimir scaling also holds for QCD with quarks. Since dynamical quarks break the center symmetry explicitly, and $N_f = 2$ QCD has a finite temperature cross over rather than a true phase transition, the thermodynamic limit of the Polyakov loop below T_c is non-vanishing.

In Figure 11 we show $(L_D^b)^{1/d_D}$ for $D = 3, 6, 8$ at all temperatures, and $D = 10, 15$ above T_c . The latter representations are too noisy below T_c to add any information. These scaled quantities are almost independent of D down to $\sim 1.5T_c$. Below this temperature we observe deviations to smaller values for the fundamental representation, whereas the values for higher D still coincide within errors. Therefore we see a violation of Casimir scaling, between the fundamental and other representations, when entering the transition region which continues to the smallest temperatures analyzed. These violations are relatively mild. Differences between $(L_D^b)^{1/d_D}$ for $D = 6$ and $D = 8$ remain statistically insignificant even at the smallest temperatures, as shown in the inset of Figure 11.

V. THE LARGE- N LIMIT

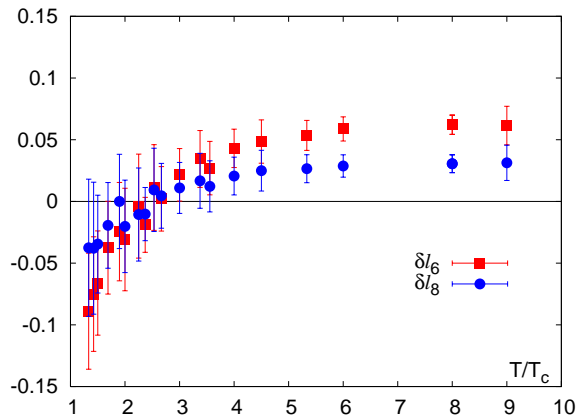


FIG. 12: Differences loops for the sextet, δl_6 , and adjoint, δl_8 .

The relation between Polyakov loops in different representations becomes rather simple in the limit of a large numbers of colors, N [8]. In this limit the expectation value of a Polyakov loop in representation D can be expressed in powers of the fundamental (L_N) and anti-fundamental, ($L_{\overline{N}} = (L_N)^*$) loop,

$$L_D = L_N^{p_+} L_{\overline{N}}^{p_-} + \mathcal{O}\left(\frac{1}{N}\right) \quad (16)$$

where the integers p_+ and p_- are determined from the Young tableaux of the representation D . We investigate this large- N factorization using our data obtained for $N = 3$.

Following [8] we analyze difference loops

$$\delta l_6 = L_6^r - L_3^r \quad (17)$$

$$\delta l_8 = L_8^r - |L_3^r|^2. \quad (18)$$

Naively, the correction terms are expected to be of the order of $(L_3^r)^2/3$, i.e., about 33%. Results, shown in Figure 12 are clearly non-zero, except at around $2.5 T_c$ where all loops are one. Our results are comparable in magnitude to those in [8] but show rather different temperature dependence. Below $2T_c$ the corrections are relatively large, and the usefulness of the large- N approximation seems doubtful. However, above this temperature, the difference loops are of order 5–10% of the loop itself, and therefore significantly smaller than the naive expectations. The large- N approximation seems to fare better than expected. This is similar to the conclusion reached for the equation of state in [6].

VI. MATRIX MODELS

One could seek effective field theories for Polyakov loops in the form of matrix models, i.e., models in which

each spatial site on the lattice, \vec{x} , contains a matrix valued “spin”, $l(\vec{x})$,

$$Z = \int \prod_{\vec{x}} dl(\vec{x}) \exp[-S_{MM}], \quad (19)$$

and the integration measure is the Haar measure. For $SU(N)$ gauge groups the matrix takes values in $SU(N)$. The action for these models can be written in the form

$$S_{MM} = -\frac{N^2}{d} \sum_{DD'} \left[\beta_{D,D'} \delta_{t(D \times D'), 0} \times \sum_{\vec{x}, \hat{n}} \text{Re} l_D(\vec{x}) l_{D'}(\vec{x} + \hat{n}) + \gamma_D \delta_{t(D), 0} \sum_{\vec{x}} \text{Re} l_D(\vec{x}) \right], \quad (20)$$

where \vec{x} runs over every site in the lattice, \hat{n} over the $2d$ nearest neighbors, l_D is the Polyakov loop in the irreducible representation D , i.e. the trace of the matrix, and $t(D)$ is the triality of the irreducible representation D . In this section we use the notation of Appendix A, i.e. traces are normalized to the dimension of the corresponding representation, D . We also use the notation $\ell_D = \langle l_D \rangle$. The constraint of vanishing triality arises from the Z_N center-invariance of the pure gauge theory.

For $SU(3)$, the effective action with only the leading term $\beta_{3,\overline{3}}$ has been investigated extensively over the years. However, when adding all irreducible representations upto a certain D , as D varies, one needs the couplings

3	$\beta_{3,\overline{3}}$	
6	$\beta_{3,6}, \beta_{6,\overline{6}}$	
8	$\beta_{8,8}, \gamma_8$	
10	$\beta_{8,10}, \beta_{10,10}, \gamma_{10}$	
15	$\beta_{3,\overline{15}}, \beta_{6,15}$	
15'	$\beta_{3,\overline{15'}}, \beta_{6,15'}, \beta_{15,\overline{15'}},$	(21)

and so on.

A matrix model would be used to obtain the loop expectation values

$$\langle l_D^r(\{\beta\}) \rangle = \frac{1}{Z} \int \prod_{\vec{x}} dl(\vec{x}) l_D \exp[-S_{MM}(l, \{\beta\})], \quad (22)$$

where $\{\beta\}$ denotes the whole set of couplings in the action. Equating these expressions to a sufficient number of observations on $\ell_D^r(T)$, one would obtain the temperature dependence of the couplings. Other predictions of matrix models, which we do not explore here, are expectation values of moments (for example, the Polyakov loop susceptibilities) and correlation functions of loops.

Note an intrinsic complication in the matching procedure. Since $\ell_D^r(T)$ is scheme dependent, the couplings that one extracts by any matching procedure must also

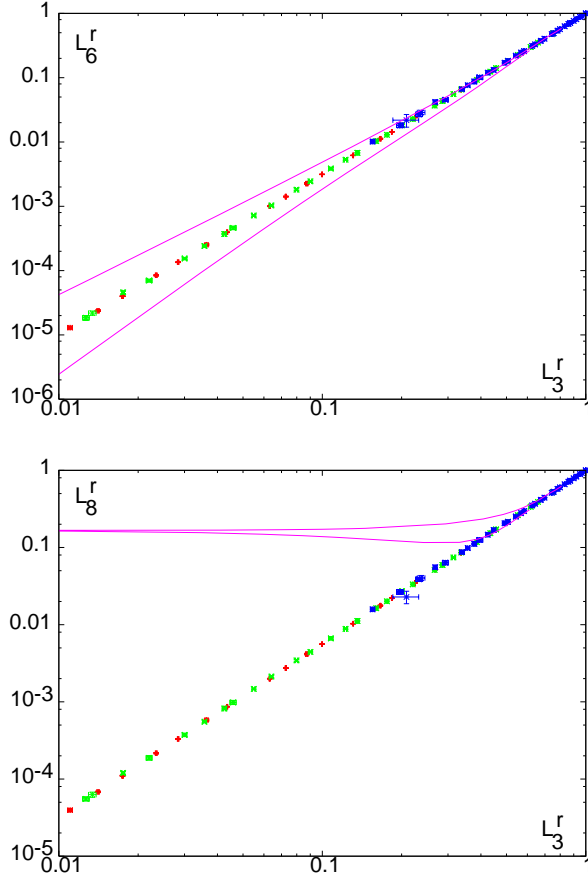


FIG. 13: Different renormalized Polyakov loops shown as a function of the fundamental loop. The fact that the data in several different renormalization schemes ($\ell_3^r(12T_c) = 0.5$ in red, 0.75 in green and 1 in blue) collapse on to a single universal curve in each case implies that there can be only a single coupling matrix model which describes this data. The line is the result of a fit using four terms in the action, as described in the text, tuned to bracket the observed curve $\ell_6(\ell_3)$.

be scheme dependent. Note also that, in order to make contact with a matrix model, one has to choose a renormalization scheme in which $\ell_D^r(T) < D$. To the best of our knowledge, these points have not been noted in the literature. Furthermore, as the number of irreducible representations increases, the number of couplings in the effective theory which need to be matched to data increases rapidly. A determination of the effective action involves extraction of the couplings through such matching at each temperature. This is an ill-conditioned problem unless the series can be cut off, and the number of couplings required is less than the number of pieces of data.

It is interesting to ask how one can bound the number of couplings needed in the matrix model. If there are C_N couplings to be determined, then C_N of the expectation

values can be traded for the couplings, and all other expectation values can be written in terms of these. For example, for a one-coupling matrix model, $C_N = 1$, one could write $\ell_D^r(\ell_3^r)$, for all $D > 3$. This relation is RG invariant: in two different renormalization schemes, if the values of ℓ_3^r at two different temperatures are the same, then the values of ℓ_D^r will be equal, for each D . For the pure gauge theory the data in Figure 13 shows that the SU(3) pure gauge theory requires a matrix model with only a single coupling. A single coupling matrix model means that ratios such as $\beta_{3,6}/\beta_{8,8}$ are fixed, and only one coupling is dependent on the temperature.

The temperature independent ratios of couplings define the shape of the universal curves, $\ell_D^r(\ell_3^r)$, and the single tunable coupling says how the curve is traversed, in a given renormalization scheme, as T changes. Therefore, one can solve the problem in two steps: first use the universal curves to fix the ratios of the couplings, and finally solve the easier problem of finding the single left over coupling. Since exact solutions for the loop expectation values are not known for matrix models with $N_c = 3$, one has to either solve the problem through a Monte Carlo simulation or in mean field theory. Here we investigate the latter option.

Taking into account the irreducible representations **3** and **6** in the effective action, one has

$$S = -3 \sum_{\vec{x}, \hat{n}} \left[\beta_{3,\bar{3}} \text{Rel}_3(\vec{x}) l_3^*(\vec{x} + \hat{n}) + \beta_{3,6} \text{Rel}_3(\vec{x}) l_6(\vec{x} + \hat{n}) + \beta_{6,\bar{6}} \text{Rel}_6(\vec{x}) l_6^*(\vec{x} + \hat{n}) \right], \quad (23)$$

where $l_6 = (l_3)^2 - l_3^*$. Using this SU(3) relation, and making a mean-field approximation, we find that

$$S = -6dV \left[\beta_{3,\bar{3}} \ell_3 \text{Rel}_3 + \frac{\beta_{3,6}}{2} \{ \ell_6 \text{Rel}_3 + \ell_3 \text{Re}(l_3^2 - l_3^*) \} + \beta_{6,\bar{6}} \ell_6 \text{Re}(l_3^2 - l_3^*) \right], \quad (24)$$

It is also possible to extend such a mean field treatment to models which include the octet representations. Using the invariance of the Haar measure, we can diagonalize the matrix, so that $l_3 = \exp(i\phi) + \exp(i\psi) + \exp[i(\phi + \psi)]$, and perform the integration over the remaining variables to give

$$dl_3 = \frac{1}{3\pi^2} \{1 - \cos(\phi - \psi)\} \{1 - \cos(2\phi + \psi)\} \times \{1 - \cos(\phi + 2\psi)\} d\phi d\psi. \quad (25)$$

Putting all this together, we find

$$Z(\beta_{3,\bar{3}}, \beta_{3,6}, \beta_{6,\bar{6}}, \ell_3, \ell_6) = \left[\int dl_3 \exp(-S/V) \right]^V = \exp[-VF]. \quad (26)$$

In the mean-field theory the expectation values are computed simply as

$$\ell_D = \frac{1}{Z} \left[\int dl_3 \exp(-S/V) \right] \text{Rel}_D, \quad (27)$$

where the ℓ_D can be expressed in terms of the angles ψ and ϕ using the formulae in eqs. (A12-A18) and the relation $\text{Rel}_3 = \cos \psi + \cos \phi + \cos(\psi - \phi)$.

Some of the results are shown in Figure 13. The observed Casimir scaling of loops implies a power-law dependence of loops on each other. The matrix model which includes only the coupling $\beta_{3,\bar{3}}$ is in fair agreement with the universal curve $\ell_6(\ell_3)$ when $\ell_3 > 1/2$. However, it disagrees with the curve for $\ell_8(\ell_3)$ already when $\ell_3 = 0.9$. By including terms in $\beta_{3,6}$ and $\beta_{6,\bar{6}}$ (in a fixed T -independent ratio to $\beta_{3,\bar{3}}$) the curve for ℓ_6 can be improved; but this leads to no perceptible change in the curve for ℓ_8 . However, by introducing the coupling $\beta_{8,\bar{8}}$, and tuning the T -independent ratio $\beta_{8,\bar{8}}/\beta_{3,\bar{3}}$, one can contrive to improve the description of the two universal curves. However the universal curves for ℓ_{10} etc., need further tuning.

The conclusion seems robust: the SU(3) pure gauge theory data can be described within a single coupling matrix model. However, it seems hard to construct a matrix model with a small number of terms which reproduces the power-law dependence of ℓ_D on ℓ_3 . The second result has been obtained within a mean field theory, and needs verification in a more complete approach, such as the full simulation of such matrix models.

VII. ADJOINT SOURCES AND GLUELUMPS

Polyakov loops in representations with non-zero triality vanish in the confined phase of the pure gauge theory, since the Z(3) symmetry of the action is realized on the states with large contribution to the path integral. The behavior of loops with vanishing triality can be different, because they are blind to the Z(3) symmetry involved in the QCD phase transition. This study is confined to the octet loop since all other triality zero loops that we constructed turned out to have very large errors below T_c .

A dynamical picture has been advanced for the behavior of adjoint Polyakov loops below T_c . An adjoint source can couple to a gluon in the medium to form a colorless composite called a gluelump. Correlations of triality zero loops can clearly be mediated by gluon exchange at any temperature, leading to screening. Gluelumps provide a summary of the main features of such screening [45] through two parameters: the free energy of separated gluelumps determines the asymptotic value of an octet Polyakov loop, the string breaking distance is the distance at which the long-distance screening behavior sets in.

We found that the bare adjoint Polyakov loop L_8^b below T_c assumes its thermodynamic limit, i.e., becomes independent of the volume for $N_\sigma^3 \times 4$ lattices with $N_\sigma \geq 24$.

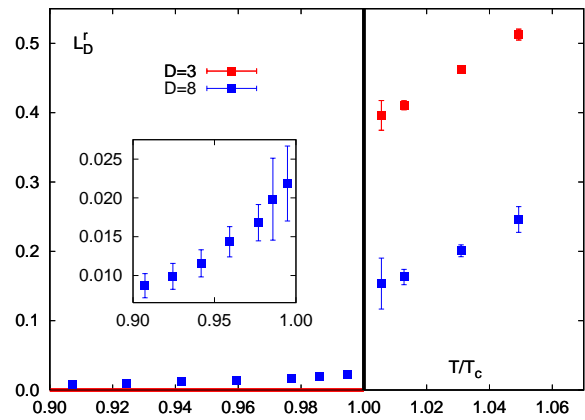


FIG. 14: The renormalized adjoint Polyakov loops below and above the critical temperature compared to the fundamental loops above T_c . The solid line below T_c indicates the vanishing fundamental loops in the confined phase.

L_8^b could be renormalized using either the $Q\bar{Q}$ method for the octet loop explained in Appendix B. However, we calculated L_8^b at more couplings than the adjoint correlator. Since we found that Z_8 agrees with Z_3 (see Appendix B), we used the $Z_3(g^2)$ given in Table II to obtain $L_8^r(T)$. Table III lists the values found for the renormalized adjoint Polyakov loop L_8^r and Figure 14 compares these results to those for the renormalized fundamental Polyakov loop, L_3^r . Although L_8^r becomes rather small below T_c , it is clearly non-zero for all temperatures analyzed by us. We observe that L_8^r rises from 0.0087(16) at $T/T_c = 0.907$ to 0.0219(48) just below T_c at $T/T_c = 0.995$. Crossing the critical temperature into the deconfined phase, L_8^r jumps almost an order of magnitude to 0.154(37) at $T/T_c = 1.005$. It is a little surprising to find the octet loop, which is blind to the Z(3) symmetry, change discontinuously at the symmetry-breaking transition. However, other triality-zero operators also change discontinuously at the phase transition, most notably the energy density. We now address the issue of string breaking and determine the binding energy of the gluelump. The specific situation at $T/T_c = 0.959$, shown in Figure 15 serves as an example. We have shown $F_{Q\bar{Q},8}^1$, and, since it becomes too noisy at large distances, also the “color average” free energy $F_{Q\bar{Q},8}$, which has the same value at long distances. These free energies clearly show that adjoint sources are screened at large distances, in clear contrast to the linearly rising free energy, $F_{Q\bar{Q},3}$ of sources in the fundamental representation. We calculate the free energy at infinite separation between the sources using the cluster property,

$$F_{8,\infty}(T) = -2T \ln L_8^r(T) = 2m_{\text{glump}}(T). \quad (28)$$

At zero temperature the energy stored in the field suffices to put on-shell two gluons from the medium and form two disjoint gluelumps [46]. At finite temperature

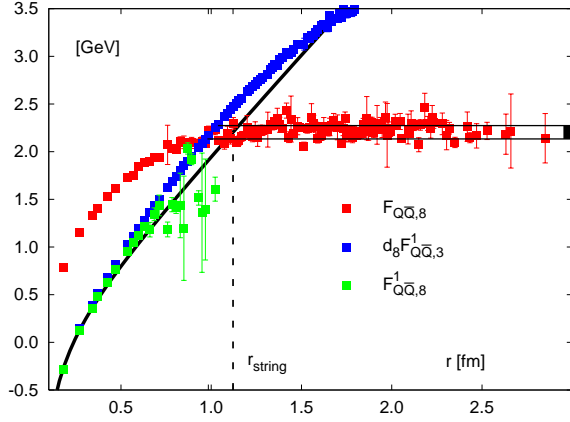


FIG. 15: Heavy quark-antiquark free energies for adjoint sources in the color singlet and color averaged channel compared to the Casimir scaled color singlet free energy of fundamental sources at a temperature of $0.959 T_c$. The dashed line indicates the definition of the string-breaking radius as explained in the text and the horizontal solid lines show the asymptotic value for the adjoint free energies. The thick black line indicates the adjoint $T = 0$ potential $V_8(r) = d_8 V_3(r)$.

this free energy can be identified with twice the gluelump screening mass.

Results for $F_{8,\infty}$ are collected in III. $F_{8,\infty}$ is shown in Figure 16 (upper panel). It changes little with T , starting from 2.331(88) GeV at $T/T_c = 0.907$ and subsequently falling to 2.06(12) GeV just below T_c . At the lowest temperatures discussed here, F_∞ indeed approaches the $T = 0$ value of $V_{8,\infty} = 2.4 - 3.0$ GeV, which is twice the mass of the gluelump obtained in [47].

We define the string breaking distance $r_{\text{string}}(T)$ by comparing the Casimir scaled free energy with fundamental sources, $d_8 F^1_{Q\bar{Q},3}$, with the screened value of the free energy with adjoint sources,

$$d_8 F^1_{Q\bar{Q},3}(r_{\text{string}}(T)) = F_{8,\infty}(T). \quad (29)$$

The results are collected in Table III. In Figure 16 (lower panel) we show the resulting values of r_{string} as a function of the temperature. There is rather mild change in r_{string} with T . It varies from 1.180(61) fm at $T/T_c = 0.907$ to 1.053(81) fm just below T_c . At the smallest temperature r_{string} almost coincides with the $T = 0$ value of 1.2 fm [48].

VIII. CONCLUSIONS

We examined the renormalized Polyakov loop in many different irreducible representations of the gauge group SU(3) in the thermodynamic limit of pure gauge QCD. It has been known for a long time that the ultraviolet divergences of the Polyakov loop can be absorbed into a multiplicative renormalization “constant” $Z(g^2)$, where

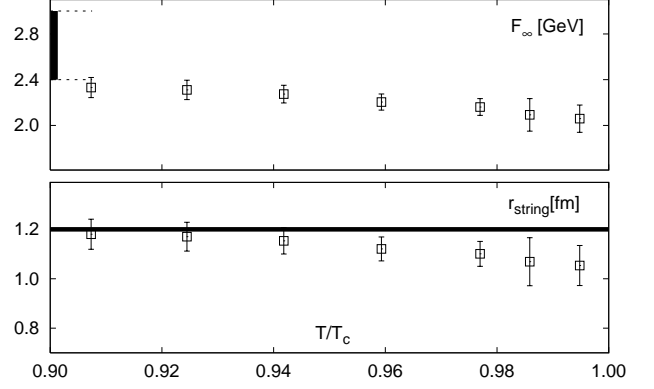


FIG. 16: Asymptotic values of the adjoint heavy quark free energies (upper panel). Estimates of the string-breaking radius using the two definitions explained in the text (lower panel).

T/T_c	F_∞ [GeV]	$r_{\text{string}}(V_8)$ [fm]	L_8^r
0.907	2.331(88)	1.180(61)	0.0087(16)
0.924	2.310(84)	1.170(58)	0.0099(17)
0.942	2.274(76)	1.153(53)	0.0116(17)
0.959	2.204(70)	1.121(48)	0.0143(19)
0.977	2.161(73)	1.101(50)	0.0168(23)
0.986	2.09(14)	1.069(97)	0.0198(53)
0.995	2.06(12)	1.053(81)	0.0219(48)
0.000	2.4 – 3.0	~ 1.2	–

TABLE III: Temperature dependence of F_∞ , string breaking distance r_{string} for the adjoint singlet free energy with respect to V_8 (see text) and the renormalized adjoint Polyakov loop L_8^r . The last line gives the values at $T = 0$ for twice the mass of the gluelump [47] and for the string breaking distance [48].

g^2 is the bare coupling. Such a renormalization factor does not depend on long distance physics, such as the temperature, T (see eq. 7). We implemented such a renormalization procedure by explicitly constructing an iteration using only explicitly gauge invariant quantities starting from a reference temperature T_{ref} incorporating this idea (see Section III B for details). This so-called direct renormalization procedure was then used to extract the renormalized Polyakov loops in representations upto the **27** of SU(3) for a wide range of temperatures (see Section II).

The technical part of our paper also consists of extending the $Q\bar{Q}$ renormalization procedure of [22] to Polyakov loops in arbitrary representations of the gauge group (see Appendix B). This is done by matching (gauge variant) correlation functions of sources in arbitrary representations to zero temperature values at the ultraviolet cut-off. Although one does not demand explicitly that the

renormalization constant depends only on the bare coupling, the matching to zero temperature in the ultraviolet makes sure that this occurs. We checked that both renormalization procedures have the same, one real parameter, freedom of choice of scheme (see Appendix C). Having two drastically different renormalization schemes which are functionally equivalent allows us not only to use the most convenient scheme in any situation, but also to cross check the results by using both schemes whenever possible. This puts the results of the lattice measurements on very strong footing. Furthermore, the equivalence of the two procedures shows that the short distance as well as the large distance parts of the heavy quark free energies obtained in Coulomb gauge become gauge independent as proposed in [49].

An interesting simplification occurs when Polyakov loop expectation values satisfy a relation called Casimir scaling (eq. 5). Then the renormalization factors in all the different representations essentially boil down to a single factor. Furthermore, large- N factorization evolves from the large- N limit of the quadratic Casimirs, and hence Casimir scaling could provide an alternative route to large- N scaling. We have presented tests of Casimir scaling in Section IV and of direct large- N factorization in Section V. Both turn out to be reasonably reliable away from T_c . However, Casimir scaling is significantly more reliable and may provide a good route to scale large- N predictions down to $N = 3$.

One subject of abiding interest is whether the high temperature phase of QCD can be described by a matrix model. We test this question in Section VI. Casimir scaling implies that there are universal (renormalization scheme independent) relations between the renormalized Polyakov loop expectation values such that all the loops we studied depend only on the value of the fundamental loop. This implies that a matrix model description could work well away from T_c . A single parameter variation of all couplings in the model would then reproduce the data on Polyakov loops, the temperature dependence of the couplings being, of course, renormalization scheme

dependent. However, it seems that a simple model with a small number of parameters is not able to reproduce the power-laws in the lattice data, at least within the mean-field analysis of the matrix model performed here.

Due to the $Z(3)$ -symmetry of the pure gauge theory, all Polyakov loops with non-zero triality vanish in the confined phase of the pure gauge theory. For the adjoint representation we have observed small, but non-zero, values below T_c for the first time in the thermodynamic limit (see Section VII). Since static adjoint sources can form bound states, called gluelumps, with dynamical gluons, correlations of adjoint loops show screening (string breaking) even in the confined phase. As a result, heavy quark free energies have a finite asymptotic value while for zero-zero triality they rise linearly with distance. Some aspects of the free energy can be captured into the phenomenology of gluelumps through a mass and radius parameter. We present results for these quantities.

Our primary technical result is the systematic development of two parallel renormalization procedures for Polyakov loops in arbitrary representations of the gauge group. This allows us to check that Casimir scaling of the renormalized loops is satisfied to good accuracy away from T_c . This is our main physical result, since it leads on to the discussion of large- N factorization and the matrix model description of lattice data.

Acknowledgment

We wish to thank J. Engels, F. Karsch, R. D. Pisarski, Y. Schröder and F. Zantow for fruitful discussions. This work has partly been supported by contract DE-AC02-98CH10886 with the U. S. Department of Energy. At an early stage of this work K. H. has been supported by the DFG under grant GRK 881/1. S. G. would like to acknowledge the hospitality of the University of Bielefeld.

-
- [1] http://www.claymath.org/millennium/Yang-Mills_Theory.
 - [2] G. 't Hooft, Nucl. Phys. **B72**, 461 (1974).
 - [3] G. Policastro, D. T. Son, and A. O. Starinets, Phys. Rev. Lett. **87**, 081601 (2001), hep-th/0104066.
 - [4] B. Bringoltz and M. Teper, Phys. Lett. **B645**, 383 (2007), hep-th/0611286.
 - [5] B. Lucini, M. Teper, and U. Wenger, JHEP **01**, 061 (2004), hep-lat/0307017.
 - [6] R. V. Gavai, S. Gupta, and S. Mukherjee, Phys. Rev. **D71**, 074013 (2005), hep-lat/0412036.
 - [7] R. D. Pisarski, Phys. Rev. **D74**, 121703 (2006), hep-ph/0608242.
 - [8] A. Dumitru, Y. Hatta, J. Lenaghan, K. Orginos, and R. D. Pisarski, Phys. Rev. **D70**, 034511 (2004), hep-th/0311223.
 - [9] A. Dumitru, J. Lenaghan, and R. D. Pisarski, Phys. Rev. **D71**, 074004 (2005), hep-ph/0410294.
 - [10] A. Dumitru, R. D. Pisarski, and D. Zschiesche, Phys. Rev. **D72**, 065008 (2005), hep-ph/0505256.
 - [11] A. Dumitru, D. Roder, and J. Ruppert, Phys. Rev. **D70**, 074001 (2004), hep-ph/0311119.
 - [12] E. Megias, E. Ruiz Arriola, and L. L. Salcedo, JHEP **01**, 073 (2006), hep-ph/0505215.
 - [13] E. Megias, E. Ruiz Arriola, and L. L. Salcedo, Phys. Rev. **D74**, 065005 (2006), hep-ph/0412308.
 - [14] C. Ratti, M. A. Thaler, and W. Weise, Phys. Rev. **D73**, 014019 (2006), hep-ph/0506234.
 - [15] P. N. Meisinger, M. C. Ogilvie, and T. R. Miller, Phys. Lett. **B585**, 149 (2004), hep-ph/0312272.
 - [16] K. Fukushima, Phys. Rev. **D68**, 045004 (2003), hep-ph/0303225.

- [17] D. Diakonov and M. Oswald, Phys. Rev. **D70**, 105016 (2004), hep-ph/0403108.
- [18] B.-J. Schaefer, J. M. Pawłowski, and J. Wambach, (2007), arXiv:0704.3234 [hep-ph].
- [19] D. Blaschke, M. Buballa, A. E. Radzhabov, and M. K. Volkov, (2007), arXiv:0705.0384 [hep-ph].
- [20] S. Ghosh *et al.*, arXiv:0710.2790 [hep-ph].
- [21] K. Kashiwa, H. Kouno, M. Matsuzaki, and M. Yahiro, (2007), arXiv:0710.2180 [hep-ph].
- [22] O. Kaczmarek, F. Karsch, P. Petreczky, and F. Zantow, Phys. Lett. **B543**, 41 (2002), hep-lat/0207002.
- [23] P. Weisz, Nucl. Phys. **B212**, 1 (1983).
- [24] P. Weisz and R. Wohlert, Nucl. Phys. **B236**, 397 (1984).
- [25] B. Beinlich, F. Karsch, E. Laermann, and A. Peikert, Eur. Phys. J. **C6**, 133 (1999), hep-lat/9707023.
- [26] B. Beinlich, F. Karsch, and A. Peikert, Phys. Lett. **B390**, 268 (1997), hep-lat/9608141.
- [27] C. R. Allton *et al.*, Phys. Rev. **D66**, 074507 (2002), hep-lat/0204010.
- [28] C. R. Allton *et al.*, Phys. Rev. **D68**, 014507 (2003), hep-lat/0305007.
- [29] A. M. Polyakov, Nucl. Phys. **B164**, 171 (1980).
- [30] V. S. Dotsenko and S. N. Vergeles, Nucl. Phys. **B169**, 527 (1980).
- [31] G. P. Korchemsky and A. V. Radyushkin, Nucl. Phys. **B283**, 342 (1987).
- [32] M. Creutz, Phys. Rev. **D23**, 1815 (1981).
- [33] E. Gava and R. Jengo, Phys. Lett. **B105**, 285 (1981).
- [34] G. S. Bali and K. Schilling, Phys. Rev. **D47**, 661 (1993).
- [35] F. Karsch, E. Laermann, and A. Peikert, Phys. Lett. **B478**, 447 (2000).
- [36] S. Gupta, Phys. Rev. **D64**, 034507 (2001), hep-lat/0010011.
- [37] O. Kaczmarek, F. Karsch, E. Laermann, and M. Lütgemeier, Phys. Rev. **D62**, 034021 (2000), hep-lat/9908010.
- [38] S. Datta and S. Gupta, Phys. Rev. **D67**, 054503 (2003), hep-lat/0208001.
- [39] U. M. Heller and F. Karsch, Nucl. Phys. **B251**, 254 (1985).
- [40] Y. Schröder, Phys. Lett. **B447**, 321 (1999), hep-ph/9812205.
- [41] G. S. Bali and P. Boyle, (2002), hep-lat/0210033.
- [42] P. H. Damgaard, Phys. Lett. **B194**, 107 (1987).
- [43] G. S. Bali, Phys. Rev. **D62**, 114503 (2000), hep-lat/0006022.
- [44] V. I. Shevchenko and Y. A. Simonov, Phys. Rev. Lett. **85**, 1811 (2000), hep-ph/0001299.
- [45] F. Karsch and M. Lütgemeier, Nucl. Phys. **B550**, 449 (1999), hep-lat/9812023.
- [46] G. S. Bali and A. Pineda, Phys. Rev. **D69**, 094001 (2004), hep-ph/0310130.
- [47] Y. A. Simonov, Nucl. Phys. **B592**, 350 (2001), hep-ph/0003114.
- [48] C. Michael, (1998), hep-ph/9809211.
- [49] O. Philipsen, Phys. Lett. **B535**, 138 (2002), hep-lat/0203018.
- [50] O. Jahn and O. Philipsen, Phys. Rev. **D70**, 074504 (2004), hep-lat/0407042.
- [51] S. Necco and R. Sommer, Nucl. Phys. **B622**, 328 (2002), hep-lat/0108008.

APPENDIX A: POLYAKOV LOOPS IN IRREDUCIBLE REPRESENTATIONS OF SU(3)

In order to obtain Polyakov loops in higher irreducible representations of SU(3) than the fundamental, we may use the theorem that the character in a direct product representation is the product of the corresponding characters, $\chi_{P \times Q}(g) = \chi_P(g)\chi_Q(g)$. Then the direct product can be reduced using the Clebsh-Gordan series to yield the Polyakov loop in various representations.

We use the following identities:

$$\mathbf{3} \times \mathbf{3} = \mathbf{6} + \mathbf{\bar{3}}$$

$$(1, 0) \times (1, 0) = (2, 0) + (0, 1) \quad (\text{A1})$$

$$\mathbf{3} \times \mathbf{\bar{3}} = \mathbf{8} + \mathbf{1}$$

$$(1, 0) \times (0, 1) = (1, 1) + (0, 0) \quad (\text{A2})$$

$$\mathbf{6} \times \mathbf{3} = \mathbf{10} + \mathbf{8}$$

$$(2, 0) \times (1, 0) = (3, 0) + (1, 1) \quad (\text{A3})$$

$$\mathbf{6} \times \mathbf{\bar{3}} = \mathbf{15} + \mathbf{3}$$

$$(2, 0) \times (0, 1) = (2, 1) + (1, 0) \quad (\text{A4})$$

$$\mathbf{8} \times \mathbf{3} = \mathbf{15} + \mathbf{\bar{6}} + \mathbf{3}$$

$$(1, 1) \times (1, 0) = (2, 1) + (0, 2) + (1, 0) \quad (\text{A5})$$

$$\mathbf{10} \times \mathbf{3} = \mathbf{15}' + \mathbf{15}$$

$$(3, 0) \times (1, 0) = (4, 0) + (2, 1) \quad (\text{A6})$$

$$\mathbf{10} \times \mathbf{\bar{3}} = \mathbf{24} + \mathbf{6}$$

$$(3, 0) \times (0, 1) = (3, 1) + (2, 0) \quad (\text{A7})$$

$$\mathbf{6} \times \mathbf{6} = \mathbf{15}' + \mathbf{15} + \mathbf{\bar{6}}$$

$$(2, 0) \times (2, 0) = (4, 0) + (2, 1) + (0, 2) \quad (\text{A8})$$

$$\mathbf{6} \times \mathbf{\bar{6}} = \mathbf{27} + \mathbf{8} + \mathbf{1}$$

$$(2, 0) \times (0, 2) = (2, 2) + (1, 1) + (0, 0) \quad (\text{A9})$$

where we have specified the irreducible representations both in terms of its dimension and through the canonical label (p, q) where p and q are integers. Recall that the maximum weight in irreducible representation (p, q) is $\mathbf{m} = \{(p+q)/2\sqrt{3}, (p-q)/6\}$, and the dimension of this irreducible representation is $D = (p+1)(q+1)(p+q+2)/2$. The notation $\mathbf{15}'$ stands for the irreducible representation $(4, 0)$, and $\mathbf{15}$ denotes the irreducible representation $(2, 1)$. Note that interchanging p and q gives the complex conjugate irreducible representation. The triality of an irreducible representation can be defined to be $t = (p - q)|_3$. In each expression above, the trialities of all the irreducible representations on the right must be equal, and must equal the sum of the trialities (mod 3) of the irreducible representations on the left. This can be used as a check.

More concretely, take the product over links and the trace defining the Polyakov loop in the $\mathbf{3}$ of SU(3),

$$l_3(x) = \text{Tr} \prod_{n=1}^{N_\tau} U_t(x + n\hat{t}), \quad (\text{A10})$$

where $l_3(x)$ is a complex number. Here the trace is normalized such that the unit matrix traces to 3. The

D	(p, q)	t	$C_2(D)$	d_D
3	(1, 0)	1	4/3	1
$\bar{3}$	(0, 1)	2	4/3	1
6	(2, 0)	2	10/3	5/2
8	(1, 1)	0	3	9/4 $\text{Im}(L_8) = 0$
10	(3, 0)	0	6	9/2
15	(2, 1)	1	16/3	4
15'	(4, 0)	1	28/3	7
24	(3, 1)	2	25/3	25/4
27	(2, 2)	0	8	6 $\text{Im}(L_{27}) = 0$

TABLE IV: Quadratic Casimir $C_2(D)$ for the representation D of $SU(3)$, $t = p - q \bmod 3$ is the triality. d_D is the ratio $C_2(D)/C_2(3)$.

Polyakov loop in an irreducible representation is the character in that irreducible representation. Hence, given the loop in one irreducible representation, that in the complex conjugate irreducible representation is obtained by complex conjugation. One specific example is

$$l_{\bar{3}}(x) = l_3^*(x), \quad (\text{A11})$$

where l^* is the complex conjugate of l . The Polyakov loop in the trivial irreducible representation $\mathbf{1}$ is unity (which gives vanishing potential in this irreducible representation). Next we construct the series of other Polyakov loops,

$$l_6(x) = l_3(x)^2 - l_3^*(x), \quad (\text{A12})$$

$$l_8(x) = |l_3(x)|^2 - 1, \quad (\text{A13})$$

$$l_{10}(x) = l_3(x)l_6(x) - l_8(x), \quad (\text{A14})$$

$$l_{15}(x) = l_3^*(x)l_6(x) - l_3(x), \quad (\text{A15})$$

$$l_{15'}(x) = l_3(x)l_{10}(x) - l_{15}(x), \quad (\text{A16})$$

$$l_{24}(x) = l_3^*(x)l_{10}(x) - l_6(x), \quad (\text{A17})$$

$$l_{27}(x) = |l_6(x)|^2 - l_8(x) - 1. \quad (\text{A18})$$

Further irreducible representations can be obtained if needed. Two of the reductions for the direct product have not been used. The Polyakov loop values in normalization used elsewhere in this paper is obtained by writing $L_D(x) = l_D(x)/D$.

APPENDIX B: $Q\bar{Q}$ RENORMALIZATION

The $Q\bar{Q}$ renormalization procedure [22] can be extended to static sources in arbitrary representations of the color group. For simplicity we will only discuss adjoint sources here in detail, but the generalization to other representations is straight forward.

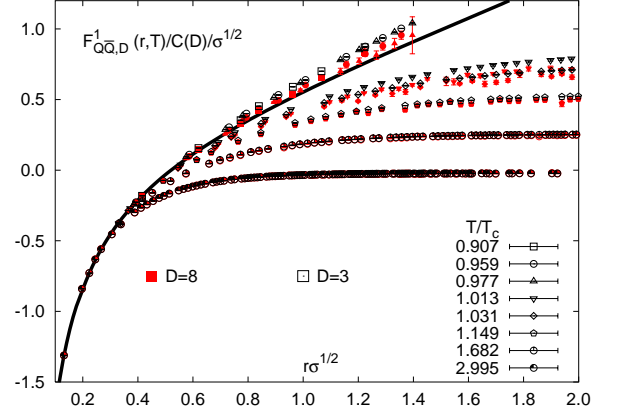


FIG. 17: Comparison of the color singlet quark-antiquark free energies for fundamental and adjoint sources scaled by the corresponding Casimir factor. The solid line represents the zero temperature potential, $V_8(r) = V_3(r)/C_2(8)$.

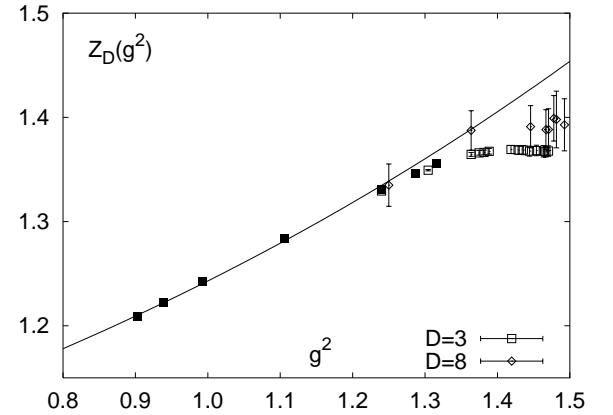


FIG. 18: The renormalization constants, $Z_D(g^2)$, for fundamental ($D = 3$) and adjoint ($D = 8$) sources plotted vs. the bare coupling $g^2 = 2N/\beta$. The solid line is the same as in fig. 4.

Given an $SU(3)$ matrix in the fundamental representation, U^3 , the corresponding adjoint matrix, U^8 , is

$$U_{ij}^8 = \frac{1}{2} \text{Tr} \left(\lambda_i U^3 \lambda_j U^{3\dagger} \right), \quad i, j = 1, \dots, 8, \quad (\text{B1})$$

where λ_i are the Gell-Mann matrices. From the hermiticity of λ_i and cyclicity of the trace all matrix elements U_{ij}^8 are real. This formula can be used to convert all link elements from the fundamental to the adjoint.

The thermal Wilson line in the adjoint representation is

$$P_8(x) = \prod_{x_4=0}^{N_\tau-1} U_4^8(\vec{x}, x_4). \quad (\text{B2})$$

Another way to define it is to take the fundamental Wil-

son line of eq. (1) and convert it to the adjoint using the prescription of eq. (B1). The adjoint Polyakov loop is the trace

$$L_8(\vec{x}) = \text{Tr} P_8(\vec{x}). \quad (\text{B3})$$

As before, we have normalized the trace such that the trace of the unit matrix is 1.

Define the correlator of two adjoint thermal Wilson lines,

$$\tilde{C}_{Q\bar{Q},8}^1(r, T) = \left\langle \text{Tr} \left(P_8(\vec{x}_1) P_8^\dagger(\vec{x}_2) \right) \right\rangle, \quad (\text{B4})$$

and $r = |\vec{x}_1 - \vec{x}_2|$. This correlator is clearly gauge dependent, and hence we define it through Coulomb gauge fixing (see [49, 50] for more on this point). The free energy with two static adjoint sources a distance r apart is

$$\tilde{F}_{Q\bar{Q},8}^1(r, T) = -T \ln \tilde{C}_{Q\bar{Q},8}^1(r, T). \quad (\text{B5})$$

Here \tilde{C} and \tilde{F} denote bare correlators and free energies; the same notation without a tilde will denote renormalized quantities.

Since the Polyakov loop is renormalized multiplicatively, the free energies are additively renormalizable. We match the finite temperature free energy to the zero temperature potential at the smallest attainable distance, a , on a lattice

$$F_{Q\bar{Q},8}^1(a, T) = \tilde{F}_{Q\bar{Q},8}^1(a, T) + 2Td_8 \ln Z_8 = d_8 V_3(a), \quad (\text{B6})$$

where $V_3(r)$ is the zero temperature potential in the fundamental representation. We use the potential derived in [51]. In the matching procedure we have used Casimir scaling of the potential at short distances. This is seen in continuum [40] and lattice [41] perturbation theory. In Figure 17 we show the renormalized quark-antiquark free energies for static sources in the adjoint ($D = 8$) and fundamental ($D = 3$) representations together with the Casimir scaled zero temperature potential $V_8(r) = d_8 V_3(r)$. The data clearly validates the assumption of short distance Casimir scaling on which the procedure rests.

Once the free energies have been renormalized at small distances, their large distance behavior is fixed. The asymptotic value can be used to define the renormalized Polyakov loop through the cluster property

$$\begin{aligned} L_D^r(T) &= \lim_{r \rightarrow \infty} \sqrt{C_{Q\bar{Q},8}^1(r, T)} \\ &= \lim_{r \rightarrow \infty} \exp \left(-\frac{F_{Q\bar{Q},8}^1(r, T)}{2T} \right). \end{aligned} \quad (\text{B7})$$

This completes the $Q\bar{Q}$ renormalization procedure for the octet loop. The requirement that Z_8 depend only on g^2 is not explicitly imposed in the $Q\bar{Q}$ renormalization procedure. However, the results, plotted in Figure 18 show

that this is obtained. The figure also shows that Casimir scaling of the renormalized Polyakov loop is obtained, since Z_8 and Z_3 agree.

Any 3×3 unitary matrix with unit determinant is uniquely specified by eight real numbers, which are coordinates in the abstract group $\text{SU}(3)$. Given these coordinates, there are canonical techniques for building matrices in any representation D which generalize eq. (B1). Hence, given the thermal Wilson line in the fundamental, one can construct the equivalent for arbitrary D . From that one can generalize every step of the procedure from eq. (B4) on for any D .

APPENDIX C: RENORMALIZATION SCHEMES

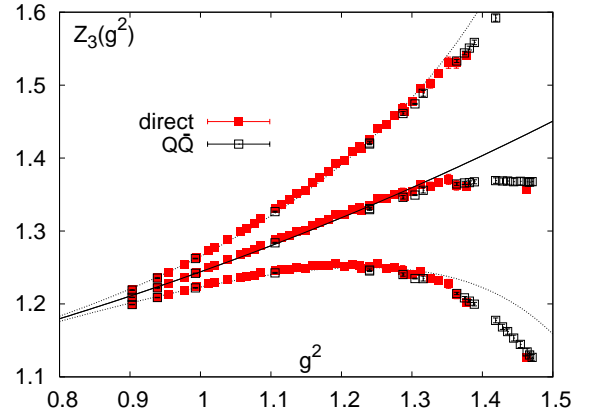


FIG. 19: Renormalization constants for fundamental loops at different scales $C = 0.0, -\sqrt{\sigma}$ (upper data points) and $\sqrt{\sigma}$ (lower data points) in (C1) from the direct and $Q\bar{Q}$ -renormalization method. The solid lines are the properly scaled fit from fig. 4.

In the direct renormalization procedure the freedom of scheme choice is the multiplicative ambiguity $L_D^r(T_{ref}) \rightarrow K_D L_D^r(T_{ref})$, for some constant K_D . This implies that at another temperature the renormalized Polyakov loop is scaled by the factor $K_D^{T_{ref}/T}$. In the $Q\bar{Q}$ renormalization procedure it is the freedom of defining the zero of the $T = 0$ potential

$$V_3(r) \longrightarrow V_3(r) + C. \quad (\text{C1})$$

Using Casimir scaling for the short distance potential, this clearly leads to the scaling

$$\begin{aligned} L_D^r(T) &\rightarrow e^{-d_D C/2T} L_D^r(T) \\ Z_D(g^2) &\rightarrow e^{-d_D a(g^2)C/2}, \end{aligned} \quad (\text{C2})$$

which incorporates Casimir scaling for the Polyakov loop. Our standard scheme choice corresponds to choosing C such that the triplet potential at $T = 0$ is given by the results of [51].

In Figure 19 we show examples of the change in renormalization scheme using the two procedures. Despite the scaling freedom, the dependence of $Z(g^2)$ on the bare coupling is independent of this scale and the temperature dependence of the renormalized Polyakov loops follow from (C2).

APPENDIX D: COLOR AVERAGE FREE ENERGIES

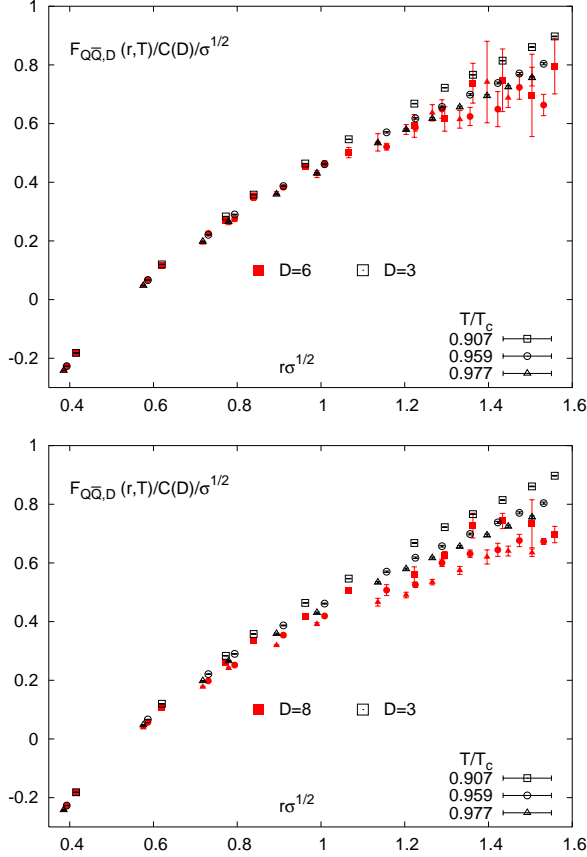


FIG. 20: Average free energies for $D = 6$ (top) and $D = 8$ (bottom) compared to the fundamental free energy below T_c .

We now turn to color averaged $Q\bar{Q}$ -free energies. Since the corresponding correlators can be obtained without a costly gauge fixing, we were able to calculate $F_{Q\bar{Q},D}(r,T)$ for representations $D = 3, 6, 8$ in the temperature range $0.9 - 3T_c$ on $32^3 \times 4$ lattices. The color average correlator for at temperature T in representation D is defined by

$$C_{Q\bar{Q},D}(r,T) = \langle L_D^r(x_1) L_D^{r*}(x_2) \rangle, \quad (D1)$$

where the star denotes complex conjugation. The color average free energy $F_{Q\bar{Q},D}(r,T) = -T \log C_{Q\bar{Q},D}(r,T)$. If Casimir scaling holds, then

$$F_{Q\bar{Q},D}(r,T)/C_2(D) = F_{Q\bar{Q},D'}(r,T)/C_2(D'). \quad (D2)$$

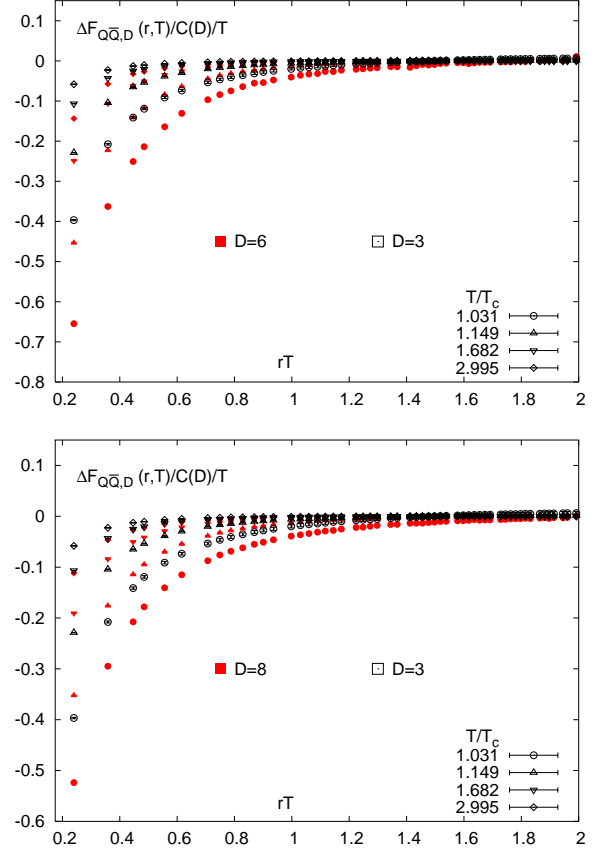


FIG. 21: Average free energies for $D = 6$ (top) and $D = 8$ (bottom) compared to the fundamental free energy above T_c .

We test this relation below and above T_c .

Below T_c we employ the renormalized average free energies

$$F_{Q\bar{Q},D}(r,T) = \tilde{F}_{Q\bar{Q},D}(r,T) + 2Td_D \ln Z_D(g^2) \quad (D3)$$

for the three lowest temperatures divided by their Casimir in fig. 20. The renormalization constants used are those found by the renormalization procedure described in sec. III C. Thus for the smallest distances all curves coincide as a consequence of the renormalization procedure. However, for all $T < T_c$ and representations $D = 6, 8$ deviations to smaller values start to show up quite early, i. e. for separations $r\sqrt{\sigma} \gtrsim 1$ for $D = 6$ and $r\sqrt{\sigma} \gtrsim 0.8$ for $D = 8$, respectively. This effect is more pronounced for the adjoint average free energy than for the sextet. The effect of string breaking sets in at larger distances than shown here and will be discussed in sec. VII.

Above T_c we compare

$$\Delta F_{Q\bar{Q},D}(r,T) = F_{Q\bar{Q},D}(r,T) - F_{Q\bar{Q},D}(r \rightarrow \infty, T) \quad (D4)$$

divided by their Casimir for the same representations $D = 3, 6, 8$ in fig. 21. We observe *screening* to take place in both higher representations. The curves for both

$D = 6$ and $D = 8$ deviate to smaller values compared to the fundamental case. We find that the ordering

$$\frac{\Delta F_{Q\bar{Q},6}(r,T)}{C_2(6)} < \frac{\Delta F_{Q\bar{Q},8}(r,T)}{C_2(8)} < \frac{\Delta F_{Q\bar{Q},3}(r,T)}{C_2(3)} < 0, \quad (\text{D5})$$

holds throughout the entire distance interval above T_c .

Thus, we conclude, that Casimir scaling (D2) is clearly violated for the average $Q\bar{Q}$ free energies in the temperature range $0.9 - 3T_c$ for the fundamental, sextet and adjoint representations.